Science of the Total Environment 572 (2016) 595–607

Contents lists available at ScienceDirect

Science of the Total Environment

journal homepage: www.elsevier.com/locate/scitotenv

Impact of hydrological alterations on river-groundwater exchange and water quality in a semi-arid area: Nueces River, Texas

Dorina Murgulet *, Valeriu Murgulet, Nicholas Spalt, Audrey Douglas, Richard G. Hay

Texas A&M University-Corpus Christi, 6300 Ocean Drive, Corpus Christi, TX 78412, USA

HIGHLIGHTS

- Hydrologic alterations in coastal rivers and semi-arid climates affect water chemistry.
- Stable isotopes of $\delta^{18}O$ and δD constrain well the magnitude of groundwater contribution.
- Variable degrees of groundwater discharge occur downstream and upstream of the dam.
- Electrical resistivity methods show sources and quality of groundwater discharge.
- Evaporation effects significantly alter surface water and groundwater quality.

GRAPHICAL ABSTRACT

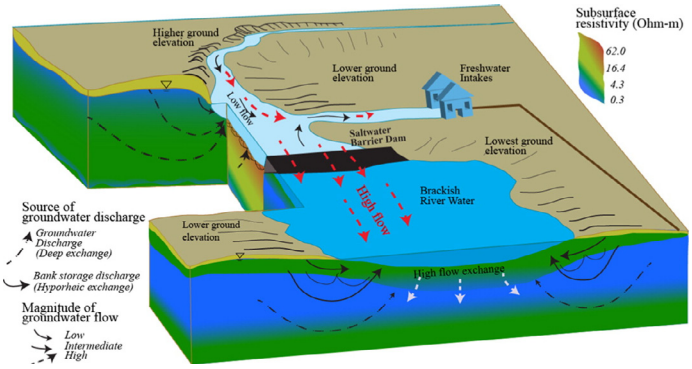

ARTICLE INFO

Article history:
Received 22 June 2016
Received in revised form 27 July 2016
Accepted 28 July 2016
Available online xxxx

Editor: D. Barcelo

Keywords:
Nueces River
Texas
Hydrologic alteration
Dam
Geochemistry
Resistivity

ABSTRACT

There is a lack of understanding and methods for assessing the effects of anthropogenic disruptions, (i.e. river fragmentation due to dam construction) on the extent and degree of groundwater-surface water interaction and geochemical processes affecting the quality of water in semi-arid, coastal catchments. This study applied a novel combination of electrical resistivity tomography (ERT) and elemental and isotope geochemistry in a coastal river disturbed by extended drought and periodic flooding due to the operation of multiple dams. Geochemical analyses show that the saltwater barrier causes an increase in salinity in surface water in the downstream river as a result of limited freshwater inflows, strong evaporation effects on shallow groundwater and mostly stagnant river water, and is not due to saltwater intrusion by tidal flooding. Discharge from bank storage is dominant (~84%) in the downstream fragment and its contribution could increase salinity levels within the hyporheic zone and surface water. When surface water levels go up due to upstream freshwater releases the river temporarily displaces high salinity water trapped in the hyporheic zone to the underlying aquifer. Geochemical modeling shows a higher contribution of distant and deeper groundwater (~40%) in the upstream river and lower discharge from bank storage (~13%) through the hyporheic zone. Recharge from bank storage is a source of high salt to both upstream and downstream portions of the river but its contribution is higher below the dam. Continuous ERT imaging of the river bed complements geochemistry findings and indicate that while lithologically similar, downstream of the dam, the shallow aquifer is affected by salinization while fresher water saturates the aquifer in the upstream fragment. The relative contribution of flows (i.e. surface water releases or groundwater discharge) as related to the river fragmentation control changes of streamwater chemistry and likely impact the interpretation of seasonal trends.

* Corresponding author at: Center for Water Supply Studies, Department of Physical and Environmental Sciences, Texas A&M University-Corpus Christi, Corpus Christi, TX 78412, USA.
E-mail address: dorina.murgulet@tamucc.edu (D. Murgulet).

http://dx.doi.org/10.1016/j.scitotenv.2016.07.198
0048-9697/

1. Introduction

Hydrological alterations, defined as any anthropogenic disruption (i.e. dam construction and river fragmentation) on the magnitude and timing of natural river flows, are one of many environmental problems affecting water resources around the world (Rosenberg et al., 2000). It is difficult, however, to distinguish the hydrological and biogeochemical effects of these alterations in areas with other types of perturbations (i.e. growing needs for water use; increased groundwater extraction reducing baseflow levels) regardless of their nature (Rosenberg et al., 2000). Research shows that in the northern third of the world, 77% of the total discharge of the 139 largest river systems is affected by river channel fragmentation due to dams, reservoirs, interbasin diversions, and irrigation (Dynesius and Nilsson, 1994). This fragmentation not only could profoundly affect the hydrology but also the biological populations over a considerable part of the world. Furthermore, the expected positive benefits of dam infrastructures to society (i.e. reduction of devastating floods, and controlled supply of water), are overshadowed in many instances by the negative environmental effects such as the reduction of freshwater flow into estuaries and ecological health declines (Olden and Naiman, 2010; Richter and Thomas, 2007; Rosenberg et al., 2000).

The major input of freshwater and the associated dissolved constituents (i.e. nutrients) to coastal estuaries come from riverine sources. However, it is important to recognize that the timing, quantity, and quality of these inflows are significant factors driving the health of estuaries and are all determined by upstream practices. For instance, altered runoff patterns and flood cycles have been shown to affect some of the biological processes attuned to seasonal cycles of climate and flow dynamics (Arthington, 2012; Weitkamp, 1994a). Francis et al. (2010) showed that the hydraulic head and the water table within an island closely emulated the river stage associated with dam releases. The drying of wetlands and upstream salt water intrusion was also associated with reduced flows due to river impairments (Weitkamp, 1994b).

The effect of water withdrawal on coastal water resources, including aquifers and estuaries, is an issue of concern worldwide (Alber and Flory, 2002). As demand for freshwater is expected to increase due to population growth (Postel, 1998), impacts on freshwater releases and reduced riverine flows are anticipated to be substantial, especially in arid and semi-arid regions where climate change will simultaneously reduce precipitation and increase evaporation (Kirtman et al., 2013). Studies in these areas indicate that elevated salinity levels in subsurface discharge to coastal waters are associated with recirculated seawater (Moore and Church, 1996; Simmons et al., 2001; Simmons, 1992). However, high evaporation rates characteristic to arid and semi-arid areas that increase the salt content in soils and bottom sediments of surface waters could play a significant role in salinization of surficial aquifers (Bighash and Murgulet, 2015; Schmidt and Garland, 2012). Beneath surface water bodies affected by evaporation with increasing salinity levels, groundwater concentrations also increase as the dense solute-concentrated waters sink into the shallow aquifers (Richter and Kreitler, 1993). The high-salt content plumes found in such systems can potentially lead to convective flow or density inversions caused by the vertically migrating fluid flow (Bauer et al., 2006; Stevens et al., 2009; Wooding et al., 1997).

In light of these pressures, the evaluation of various flow regimes and climatic conditions for sustainable river management and the analysis of the environmental effects of hydrologic alteration are both areas of active investigation (Poff et al., 1997; Sparks, 1992). As the exchange between groundwater and surface water and its linkages to freshwater availability are seldom considered in planning decisions, the potential for disturbances originating from human activity may be substantial. The purpose of this study is to understand the effects of saltwater barriers and environmentally regulated freshwater releases in an impaired coastal stream that is subject to long-term droughts and sporadic flooding. More specifically, this study aims to show the effects of hydrologic impairments on the groundwater–surface water exchange and geochemistry of surface and interstitial water.

Chemical composition of river waters is generally controlled by inputs from rain water and runoff, water-rock interaction, and anthropogenic activities (Han and Liu, 2004). Although recent studies recognize the role of groundwater on many aspects of river processes (Cook, 2013; Sear et al., 1999), few studies have attempted to analyze the groundwater-surface water signal in the hydrology and water chemistry of impaired rivers and the degree of interaction, suggesting that this area merits further research. Multiple methods have been utilized to investigate the contribution of groundwater to surface water in rivers such as mathematical models (Frei et al., 2009), geochemical tracers, statistical methods (Cable et al., 2004; Su et al., 2012), and seepage meters (Lee, 1977).

The most commonly used point measurements make it difficult to upscale the results due to subsurface and streambed heterogeneities (Cook, 2013; Kalbus et al., 2006). Application of radon (^{222}Rn; half-life ($t_{1/2}$ = 3.8 d)) as a geochemical tracer has proven to be successful in detecting and quantifying groundwater discharge rates to surface waters (Burnett and Dulaiova, 2003; Moore, 1996; Peterson et al., 2008) offering an integrated signal over larger extents. A naturally occurring inert gas, commonly found in soils and subsurface sediments/rocks, and the product of radium decay (Crusius et al., 2005), radon is abundant in groundwater in relation to surface waters (Burnett, 2003). Although these properties make radon an ideal tracer of groundwater discharge, further constraints on groundwater sources are necessary to determine the groundwater contribution to surface waters (Li et al., 2009). Recently, novel subsurface imaging techniques such as the direct current electrical resistivity tomography (ERT), acquired as either continuous resistivity profiles (CRP) or time-lapse, have been increasingly used to delineate and quantify groundwater flow paths and discharge rates into surface water bodies over large spatial extents (Bighash and Murgulet, 2015; Cardenas and Markowski, 2010; Cardenas et al., 2010; Green et al., 2008; Greenwood et al., 2006; White, 1988).

For the purpose of this study a unique combination of traditional (i.e. geochemical modeling and major and trace element molar ratios) and novel (i.e. electrical resistivity and environmental isotope tracers) techniques are utilized. Geochemical modeling using PHREEQC, which offers a comprehensive means of understanding a variety of reactions and processes in natural waters (Parkhurst and Appelo, 2013), was applied to quantify the groundwater and seawater contribution to river water. Ionic mass ratios complemented by stable isotopes and ^{222}Rn have been utilized to examine sources and processes affecting river waters under different hydrologic conditions. In combination with continuous resistivity profiling (CRP), this study offers a unique approach that can be applied in other areas to understand the effects of hydrologic impairments on water resources and evaluate the interaction between groundwater and surface water.

2. Study area

Nueces River (NR), located on the South Texas Gulf coast, is one of the main sources of freshwater to nearby communities and to the Nueces Bay. It is threatened by water quality degradation, specifically pertaining to increased total dissolved solids (TDS) and salinity concentrations in areas adjacent to Hazel Bazemore Park (HBP) and downstream of the Calallen saltwater reservoir dam (referred in this paper as the saltwater barrier) (Fig. 1). Almost 98% of the river flows are controlled by the Choke Canyon Reservoir and Lake Corpus Christi dam system (Fig. 1) which provides water to the City of Corpus Christi, San Patricio County Municipal Water Districts, and others (NBBEST, 2011). Due to these water demands and implemented management practices to meet environmental inflows, the lower part of the river has experienced extensive hydrological alterations. Major modification and channelization redirecting flow away from the bay towards the

Rincon Bayou (i.e. intake located upstream of the saltwater barrier) as well as limited releases from the Lake Corpus Christi dam (Fig. 1) have changed the flow regime, ecology, and fluvial forms. Previous studies have attributed reductions in riverine freshwater inflows of ~55% to the bay and ~99% to the delta (Fig. 1) to these alterations and drought (USDI, 2000). The river stretch below the saltwater barrier (Fig. 1) - is generally stagnant or very slow flowing as it does not receive any upstream flow during periods of low precipitation and/or no upstream releases as shown in Fig. 2.

The hydrogeology of the area consists of both confined and unconfined aquifers in a layered stratigraphy of alternating and intermixed lenses of silt, clay, sand, and gravel (Shafer, 1968). Nueces Bay falls within a subsection of the Gulf Coast Aquifer system, a leaky artesian aquifer comprised of a complex of clays, silts, sands, and gravels forming the Chicot, Evangeline, and Jasper aquifers (Ashworth and Hopkins, 1995; Chowdhury et al., 2004). Corpus Christi Bay and the surrounding systems are generally in direct contact with the Chicot aquifer, which is the shallowest of the mentioned aquifers. The direction of groundwater flow in this aquifer is in general towards the river and bay (Fig. 1). The stratigraphic units of the Chicot aquifer consist of an overlying alluvial formation preceded by the Beaumont and Lissie formations (Ashworth and Hopkins, 1995), which are generally composed of clays and clayey silts with intermittent sand and gravel lenses that continue out into the Gulf of Mexico (Chowdhury et al., 2004).

Most of south Texas is underlined by saline groundwater (>1000 mg/L total dissolved solids (TDS)) at depths <150 m below land surface (Richter et al., 1991). High saline areas occur locally throughout South Texas (Feth, 1965). In the study area groundwater quality varies spatially and with depth: in the central and northeastern parts of the aquifer groundwater exhibited total dissolved solids (TDS) concentrations of <500 mg/L while it is gradually increasing to >10,000 mg/L to the south (George et al., 2011; Shafer, 1968). Given the presence of rich natural uranium sandstone deposits within the Texas Coastal Plain region, groundwater is highly enriched in radium and radon (George et al., 2011). Water quality in the Nueces River basin generally contains high dissolved solids concentrations during low flow, in which sodium and chloride predominate while during the short periods of high flow, dissolved solids concentrations are low and calcium and bicarbonate are the principal constituents (Kunze, 1971).

3. Methods

To constrain hydrologic conditions during sampling events, we used the hourly data collected from two automatic river gauges (available from http://waterdata.usgs.gov/tx/nwis) located in close proximity to two of the hydrologic impairments, as shown in Fig. 1. Specific conductance (SC) and precipiation depths (available from http://www.cbi.tamucc.edu/cbi/data/) were also included from stations located in the upstream portion of the river (NRU; Fig. 1) and are depicted in Fig. 2.

3.1. Aqueous samples

Aqueous samples were collected from the water column and interstitial water. Field parameters (i.e. conductivity, pH) were collected at the time of sampling using a multi-probe YSI series 6 sonde. Surface water samples were collected using a Van Dorn bottle from approximately 0.2 m above the sediment-water interface and 0.2 m below the water-air interface. Pore water samples were aquired using a peristaltic pump attached by tubing to an AMS retract-a-tip piezometer sampler with a screen length of 5 cm inserted ~0.3–1 m into the sediment (Charette and Allen, 2006). The tubing was flushed with sample water at least three equivalent volumes of the inside tubing space before

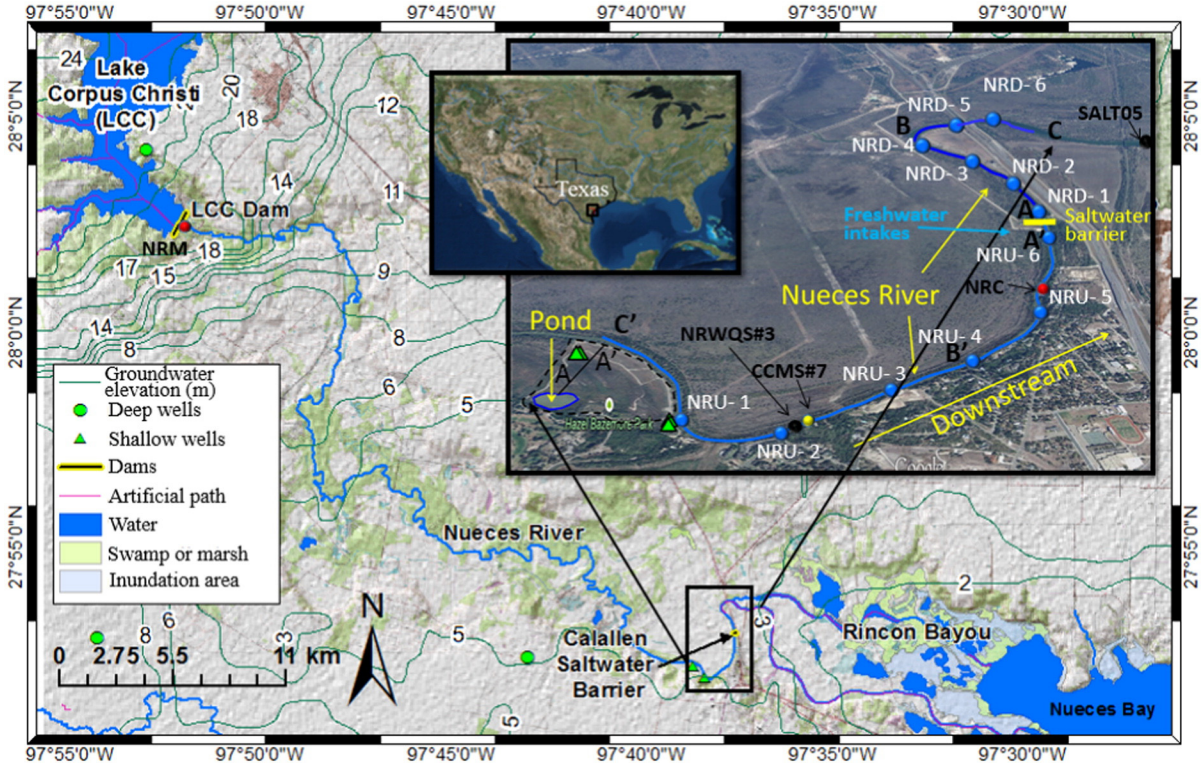

Fig. 1. Geographic location of study area and sampling stations located upstream (NRU) and downstream of the saltwater barrier dam (NRD) and shallow and deep groundwater (two of the six samples are located below the inset map and slightly further north). Location of the evaporation pond, saltwater barrier dam, and freshwater intakes are included in the upper right corner inset map. This inset map depicts the location of land ERT surveys: profile line A–A′ and the resistivity map (EM31) area represented by the dashed lines at Hazel Bazemore Park and the CRP transects depicted by blue lines along transects A–B–C (downstream of the saltwater barrier) and A′–B′–C′ (upstream of the dam). Included are also the locations of the Corpus Christi Meteorological Station # 7 – CCMS#7 (yellow dot), water quality stations: SALT05 and Nueces River Water Quality Station # 3 – NRWQS#3 (black dots), and stream gauges: Nueces River at Calallen (NRC) and Mathis (NRM)) (red dots). (For interpretation of the references to color in this figure legend, the reader is referred to the web version of this article.)

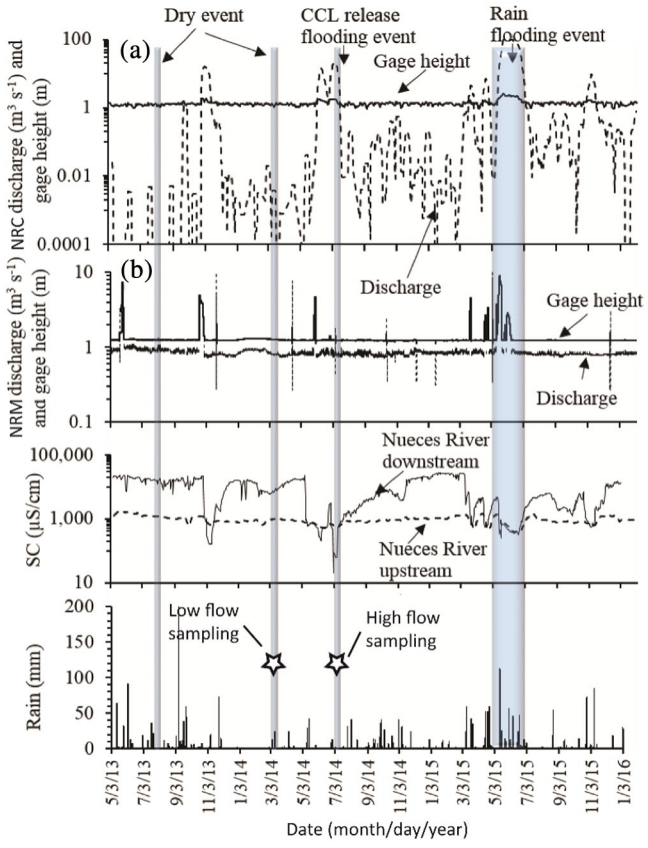

Fig. 2. Comparison graph of Nueces River discharge and gage height from stream gauges: Nueces River at Calallen (a) and Mathis (b); specific conductance (SC) from water quality stations: SALT05 and Nueces River Water Quality Station # 3 (c); and precipitation depth data from the Corpus Christi Meteorological Station # 7(d). Geographic location of these stations is depicted in Fig. 1. Vertical bars represent examples of dry events, increased river discharge due to environmental releases from LCC Dam and due to high precipitation rates. Sampling times for this study are noted by stars. Note the long period of extremely low or no precipitation before March 2014 (low flow sampling event) and July 2014 (high flow event). Also noteworthy is that during low flow conditions the SC of the NRD is an order or two of magnitude higher than that of NRUand that SC in NRD is much lower during the CCL environemntal release in June–July 2015 than that during the high precipitation event in May–June 2015.

each sample collection to avoid cross-contamination. Water samples were collected from four monitoring wells with screened depths ranging from 5 to 10 m and located along the river banks, upstream of the saltwater barrier (Fig. 1) representing the shallow groundwater endmember. Six samples were also collected from wells located further inland representing the deeper groundwater endmember. Samples were aquired at the wellhead after purging at least three well volumes or until all YSI readings were stable.

All water samples were analysed for ions such as chloride (Cl^-), sulfate (SO_4^{2-}), bromide (Br^-), calcium (Ca^{2+}), sodium (Na^+), magnesium (Mg^{2+}), manganese (Mn^{2+}) (Andres et al., 2006), etc., stable isotopes of oxygen ($\delta^{18}O$), hydrogen (δD), and carbon ($\delta^{13}C$ of dissolved inorganic carbon (DIC)), and radon (^{222}Rn). Abundances of stable isotopes are reported in the conventional delta (δ) notation in per mil (‰). DIC concentrations are reported in moles/liter (mol/L) while $\delta^{18}O$ and δD measurements are reported relative to the Vienna Standard Mean Ocean Water (VSMOW) and $\delta^{13}C$ are relative to the Vienna Pee Dee Belemnite (PDB) carbonate standard. Standard deviation and precision of $\delta^{18}O$, δD, and $\delta^{13}C$ measurements are ± 0.1‰ (1σ), ± 1.0‰ (1σ), and ± 0.3‰ (1σ), respectively, based on sample replicates and internal and international standards.

Major anions (i.e. Cl^-, Br^-, and SO_4^{2-}) were measured using a Dionex High Performance Ion Chromatograph (Model DX600, Dionex Corp., Sunnyvale, California) equipped with an autosampler, an anion-exchange column (7 mm; 4 × 250 mm; Dionex AS14A), and a conductivity detector (Dionex CD25). The detection limit of the method ranged between approximately 0.05 (for Br^-) and 0.1 mg/L (Cl^- and SO_4^{2-}) depending on the the background signal of measured constituents in the samples with a precision of ± 0.01 mg/L (1σ). Cation measurements were conducted using the inductively coupled plasma mass spectrometer (ICP-MS) with detection limits at or below the single part per trillion (ppt) level dependent on the element.

Samples for ^{222}Rn in water were collected in 250 mL or 2 L bottles with no head space according to methods developed by Durridge Co., Inc. (Big Bottle System). Durridge RAD-7 radon-in-air detector with RAD AQUA accessories and a drystik was used to measure ^{222}Rn concentrations in surface, porewater and groundwater and for continuous measurements in surface water (Durridge Co., Inc. Rad-7, RAD AQUA). Continuous measurements of ^{222}Rn and time-lapse resistivity imaging were collected at one location above the saltwater barrier to provide a proof-of-concept of potential pulses of SGD as they occur.

3.2. Geochemical data analyses

Correlations between major element concentrations and molar and stable isotope ratios were used to characterize surface water signatures in relation to groundwater and seawater. Both shallow and deeper groundwater characteristics were used in the analyses. Seawater geochemical characteristics for stable isotopes, DIC, SO_4^{2-}, Br^- and Cl^- signatures were derived from the closest seawater source which is Nueces Bay (Fig. 1) while for all other constituents (e.g. Ca^{2+}, and Mg^{2+}), the typical seawater composition reported in literature (Culkin, 1965) was used. Most analyses are based on two or three end-member mixing models which were identified based upon the chemical and isotopic compositions of surface water, seawater, and groundwater. Endmember concentrations were calculated as the average of different sample sizes such as: four shallow groundwater, six deeper groundwater, up to 24 surface water, and up to 12 for porewater.

Speciation and saturation index (Sasamoto et al., 1999) calculated using the PHREEQC Interactive Version 3.1.2.8538 (Parkhurst and Appelo, 2013) were used to quantify groundwater contribution to the river under both investigated hydrologic conditions. Chloride concentrations were used as the constraining end-member given the elevated concentrations of shallow grundwater and the evaporation effects. Solution saturation indexes with respect to solid phases (i.e. calcite, and kaolinite) were computed using the following Eq. (1) using aqueous speciation of the sample calculated using the equilibrium geochemical speciation/mass transfer model PHREEQC (Parkhurst and Appelo, 2005). Mixing models developed using the calcite SI and the Cl concentration of the fresh surface water, shallow groundwater, and deep groundwater as end-members were used to estimate the potential contribution of groundwater to surface water and mixing effects. The two groundwater end-members were considered given the significant differences in their geochemical composition.

3.3. Resistivity

Collection of continuous resistivity profiles (CRP) of the subsurface on the upstream portion of the river were conducted during March and July 2014. Due to instrument malfunction, CRP images were collected only in March 2014 for the downstream portion of the river. Land ERT profiles were collected in March 2014 in close proximity to the upstream river banks (at Hazel Bazemore Park), using a Stratagem EH4 Electrical Conductivity Imaging System and an *AGI SuperSting R8 Marine* (8-channel) resistivity profiler. Water table resistivity mapping was also collected in March 2014 for the area surrounding the monitoring shallow wells and an evaporation pond at the Hazel Bazemore Park (Fig. 1) using and an Electromagnetic (EM) 31 Resistivity Imaging System. These images were used to characterize the subsurface hydrostratigraphy (Nyquist et al., 2008) and pore fluid conductivity/

resistivity (Loke, 2011) as well as delineate potential flowpaths and groundwater-surface water interaction zones.

Marine profiles or CRPs, which are continuous resistivity measurements of the water column and the subsurface sediments, were complemented by GPS positioning and depth profiles. The *AGI SuperSting R8 Marine* (8-channel) resistivity profiler imaging system used for this study is paired with a 112 m cable with 56 electrodes spaced 2 m apart. During collection of CRPs the electrode cable was towed behind a boat along approximately two miles above and below the saltwater barrier dam (Fig. 1) while current is injected every 3 s along the moving path and 8 apparent resistivity measurements, representing 8 depth levels, are read for each current injection and the data are continuously recorded and stored by the *SuperSting*. Furthermore, three time-lapse resistivity (ER) images were collected over a period of 7 h at one selected location upstream of the dam (Fig. 1) with the resistivity cable deployed at the water surface along the 112 m streamer. For stationary (land and marine) surveys, the cable is kept in place during the duration of measurement. Depth of penetration for all types of measurements depends on length of the cable and array type (typically approximately 20% of the electrode spread length) (Advanced Geosciences, Inc.) which for this system is up to 19–20 m.

Each individual electrical resistivity image was gathered into a continuous dataset or tomograph and then inverted to earth model resistivity values using the 2D AGI EarthImager with the maximally smooth least squares algorithm (Loke, 2011; Samouëlian et al., 2005). Field observations on river water conductivity and thickness of the water column below the electrode array were applied in the inversion to constrain the results so that changes in surface water conditions do not affect the resistivity model results for the underlying sediment below the electrode array (Nyquist et al., 2008). The resolution of subsurface materials acquired using resistivity imaging systems such as the *Marine SuperSting R8*, is much higher than those of other geophysical methods (Swarzenski et al., 2006). Uncertainties associated with electrical resistivity data inversions are also much lower and the ability to measure changes in resistivity at such a small scale facilitates more accurate visual interpretations of subsurface sediment and interstitial fluid chemistry. Thus, the electrical resistivity measurements employed in this study help capture at a higher resolution pore fluid quality and aquifer substrate-related characteristics, both below land surface and sediment-water interface (Cardenas and Markowski, 2010; Viso et al., 2010).

4. Results and discussion

4.1. Geochemistry data analysis

4.1.1. Stable isotopes

4.1.1.1. Oxygen and hydrogen stable isotopes. Spatial and temporal variation of $\delta^{18}O$ and δD abundances of river waters are generally driven by multiple factors such as geographical and climatic (i.e. latitude, elevation, distance from the coast, humidity, temperature, precipitation, evaporation) and addition or removal by exchange with groundwater (Price et al., 2008; Walther and Nims, 2015 (Price, 2008 #104)). At low flow, NRU porewater $\delta^{18}O$ and δD ratios spanned from −3.1 to 0.5‰ (mean −1.1‰ and −18.8 to −0.5‰ (mean −8.1‰), respectively, with two signatures more depleted than surface water while the rest (i.e. four samples) were more enriched, comparatively (Fig. 3a). Except for station 2, surface water isotope abundances were nearly similar along the sampling transect, with $\delta^{18}O$ and δD ranges: −1.9 to −1.3‰ (mean −1.7‰) and −10.9 to −7.7‰ (mean −8.1‰), respectively. The high flow event yielded slightly more depleted $\delta^{18}O$ and δD signatures. Contrary to the low flow condition, porewater exhibited the most depleted ratios (−4.0 to −1.3‰ (mean −2.6‰) and −22.3 to −7.1‰ (mean −14.4‰)) while surface water (−0.6 to −0.5‰ (mean −0.6‰) and −2.5 to −2.5‰ (mean −2.4‰)) was enriched above the average shallow or deep $\delta^{18}O$ and δD groundwater signatures (average $\delta^{18}O$ and δD: −1.9‰ and −12.2‰ and −5‰ and −27‰, respectively). (Fig. 3a). Most of the enriched isotopic signatures in porewaters were measured at stations NRU-5 and 6 located in closest proximity to the saltwater barrier. While this enrichment could signify more water input from bank storage, it could also reflect a slight influence of evaporation on stagnant water upstream the barrier, especially during the dry/low flow event. However, the evaporation effects were not as high as it would be expected for stagnant water (Walther and Nims, 2015) given the significant uptakes of freshwater at this location (Fig. 1). The isotopically depleted porewater signatures noted for both hydrologic conditions, and especially at high flow, cannot be explained by a riverine source or input of groundwater from near-bank storage (i.e. shallow groundwater) which in most instances were more enriched than dry weather/low flow signatures of river water. Contribution from deeper and longer flowpaths of groundwater recharging within distant aquifer outcrops with characteristically more depleted abundances of these stable isotopes (range of $\delta^{18}O$ and δD means: −5.2 to −4.4‰ and −26 to −30‰ (Young et al., 2014), respectively) likely explain the more depleted porewater signatures.

At low flow, NRD $\delta^{18}O$ and δD ratios were much more enriched than the upstream river. While surface water signatures (−0.9 to −0.7‰ (mean −0.8‰) and −5.4 to −4.2‰ (mean −4.8‰)) plot close to some of the shallow groundwater, porewater samples (−0.7 to 2.9‰ (mean 1.7‰) and −5.5 to 14.8‰ (mean 7.5‰)) were much more enriched in both heavy isotopes of oxygen and hydrogen (Fig. 3b). This magnitude of enrichment can be explained by the Rayleigh Equilibrium Isotope fractionation process during evaporation of high salt content waters or residual brines when the δD and $\delta^{18}O$ ratios become more enriched as more of the isotopically depleted $H_2^{16}O$ enters the vapor phase (Craig et al., 1963; Lloyd, 1966). Walther and Nims (2015) found that limited dilution of downstream waters due to reduced inflows caused by upstream impairments are likely to enhance evaporative processes taking place over the course of a drought.

During high flow conditions, $\delta^{18}O$ and δD isotopic abundances were more homogeneous showing little differences between surface water and porewater. Overall, surface water $\delta^{18}O$ and δD isotopes were slightly more enriched when compared to the low flow event (−0.4 to −0.5‰ (mean −0.5‰) and −1.3 to −1.9‰ (mean −1.6‰), respectively) while porewaters were more depleted (−0.6 to 0.3‰ (mean −0.3‰) and −2.3 to 2.1‰ (mean −0.8‰), respectively) and more similar to the surface water signatures (Fig. 3b). Furthermore, no significant differences among surface water abundances of these isotopes were noted for the two river fragments (NRU and NRD) showing a common source of recharge derived from upstream environmental releases.

4.1.1.2. Dissolved inorganic carbon isotopes. NRU DIC concentrations and $\delta^{13}C$ abundances during low flow ranged from 1.2 to 6.2 mol/L (mean 2.7 mol/L) and −8.7‰ to −3.9‰ (mean −7.2‰), respectively. Comparatively, high flow (i.e. July) yielded higher DIC concentrations and highly depleted observed $\delta^{13}C$ abundances, ranging from 3.3 to 12.7 mol/L (mean 5.4 mol/L) and −29.8 to −8.6‰ (mean −13.0‰), respectively. These trends are generally attributed to microbial activities (Fig. 4a) within more oxidizing sediments (Hellings et al., 2000; Presley and Kaplan, 1968) that likely intensified between March and July due to increases in temperature and input of more reducing groundwaters (i.e. upwelling of deeper groundwater as indicated by the oxygen and hydrogen isotopes (Fig. 3a)) (mean porewater DIC and $\delta^{13}C$ were 10.6 mol/L and −21.4‰, respectively).

Similar to the upstream stretch, low flow conditions-DIC concentrations for NRD were also in the lower range (1.5 to 7.1 mol/L; mean 3.3 mol/L). Although also more enriched, $\delta^{13}C$ abundances show more variation (−13.2 to 0.3‰; mean −7.8‰) than the upstream river, comparatively, revealing the influence of both biological and geochemical influences for the lower, mostly stagnant part of the river. At high

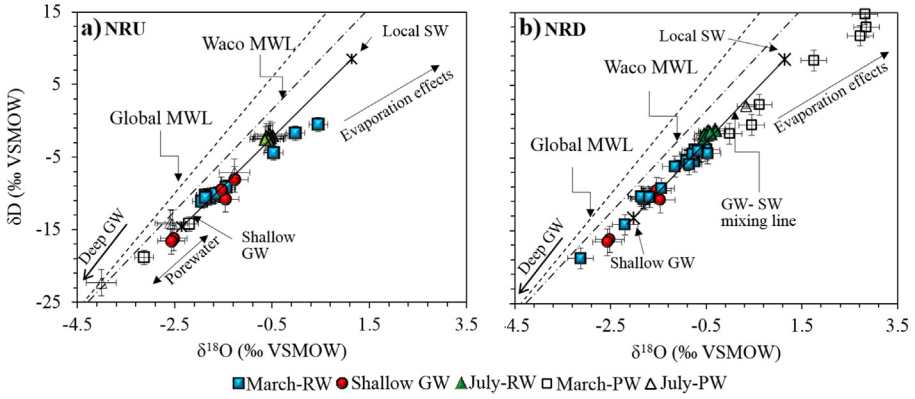

Fig. 3. Cross-plot of the low (March) and high (July) flow $\delta^{18}O$ and δD of porewater, surface water, and shallow groundwater (GW) data for upstream (a) and downstream (b) Nueces River. (includes standard error bars). All isotope data plot below the Waco (Texas) meteoric water line (Waco MWL) (data available from the International Atomic Energy Agency http://www-naweb.iaea.org/napc/ih/IHS_resources_gnip.html) which is included as a reference for recharge of deep groundwater and the Global MWL (Craig and Gordon, 1965). The data plot, however along the shallow groundwater-seawater mixing line except for a few low flow NRU surface waters (a) and most low flow NRD porewaters (b), showing effects of evaporation. Note the shift in NRU samples, namely low flow surface water and all porewater towards more depleted abundances and closer to the Waco MWL hinting at a more distance source of groundwater discharge (i.e. deep groundwater).

flow, DIC concentrations were slightly higher in surface water (mean 3.0 mol/L), but not as enriched in porewater (mean 6.8 mol/L) as noted for the upstream portion (Fig. 4b). When compared to low flow, $\delta^{13}C$ signatures were slightly more depleted (−18.1 to −5.5‰; mean −9.2‰) but not as depleted as in the upstream portion. Since the high flow sampling event follows an extensive period of drought (Fig. 2) and high temperatures, it is expected that the signature of the interstitial water for both river stretches between the two sampling events to be affected by bacterial activities as the sediments become anoxic. As a result of bacterial activities, DIC concentrations were observed to increase while the $\delta^{13}C$ ratios decreased. Although at a maximum height and discharge during the July/wet event (Fig. 2), surface water, especially NRU, seems to be slightly influenced by the porewater geochemistry, likely as a result of groundwater upwelling or benthic fluxes.

4.1.2. Na^+/Cl^- and SO_4^{2-}/Cl^- molar ratios

4.1.2.1. Upstream river. During both low and high flow conditions, concentrations of Na^+, Ca^{2+}, Mg^{2+}, Cl^-, and SO_4^{2-} (Table S1, Supplementary inf.) were generally one order of magnitude higher in porewater when compared to surface water and lower in average when compared to shallow groundwater. The molar ratio of sodium to chloride (Na^+/Cl^-) in porewater during low flow conditions was, with one exception, greater than that of seawater and the 1:1 ratio associated with halite dissolution (i.e. 1.0) (Krishnaraj et al., 2011). All surface water samples showed enrichment in Na^+ compared to the seawater signature and most had Na^+/Cl^- ratios above that of typical halite dissolution which can be explained by silicate weathering reactions (i.e. albite weathering) (Meybeck, 1987). Enrichment of sodium over chloride above levels explained by halite dissolution was also evident in the shallow and deeper groundwater (Fig. 5a).

With one exception, the molar ratios of sulfate to chloride (SO_4^{2-}/Cl^-) for porewaters were lower than the seawater ratio and much lower than the shallow and deep groundwater (Fig. 5b). SO_4^{2-} consumption in the interstitial water was likely caused by microbial reduction processes which also result in depleted $\delta^{13}C$ of DIC ratios as indicated in Section 4.1.1.2. Significant production of SO_4^{2-} was only observed at station NRU-2 with a signature similar to that of shallow groundwater sampled along the river bank (Figs. 1, 5b). This extent of enrichment of SO_4^{2-} over Cl^- has been associated with microbial dissolution of iron sulfate (FeS_2) minerals or desorption of SO_4^{2-} from sediments as favored by changes in the local redox conditions (Jones et al., 2006). Enrichment of SO_4^{2-} above the seawater ratio was also noted in surface water but to lower degrees, similar to the deeper groundwater.

High flow porewater SO_4^{2-}/Cl^- ratios were in average lower than at low flow showing a slight growth in consumption of SO_4^{2-} compared to seawater and groundwater, likely augmented by microbial reduction processes during the dry period preceding upstream water releases (i.e. pre-flooding drought conditions). As noted in Fig. 5b, with depletion of SO_4^{2-} in the sediment, surface water ratios were also decreasing

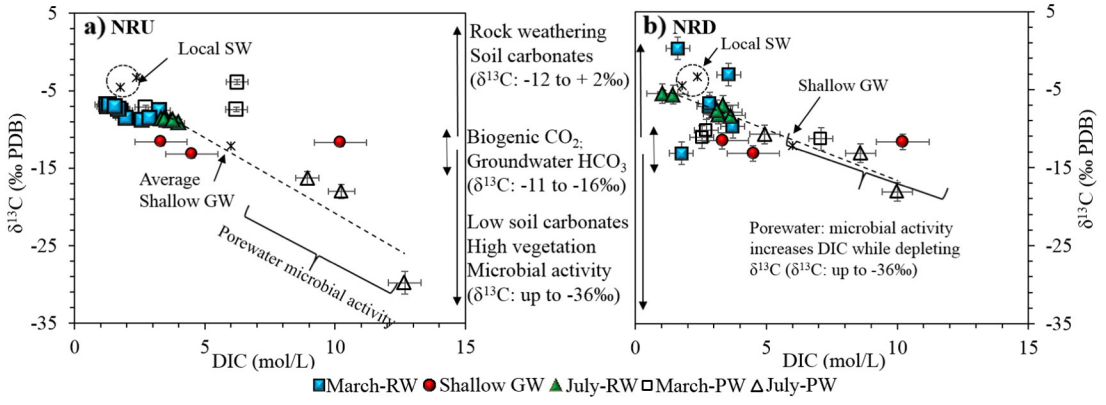

Fig. 4. Cross-plot of the low (March) and high (July) flow $\delta^{13}C$ and DIC of porewater, surface water, and shallow groundwater (GW) data for upstream (a) and downstream (b) Nueces River (includes standard error bars). Note the depleted $\delta^{13}C$ abundances and higher DIC concentrations of July porewaters for both NRU and NRD likely reflecting the influence of microbial activity. Other porewaters showed similar characteristics to groundwater and surface water exhibited signatures reflecting weathering of minerals as also indicated by the Na^+/Cl^- and SO_4^{2-}/Cl^- ratios.

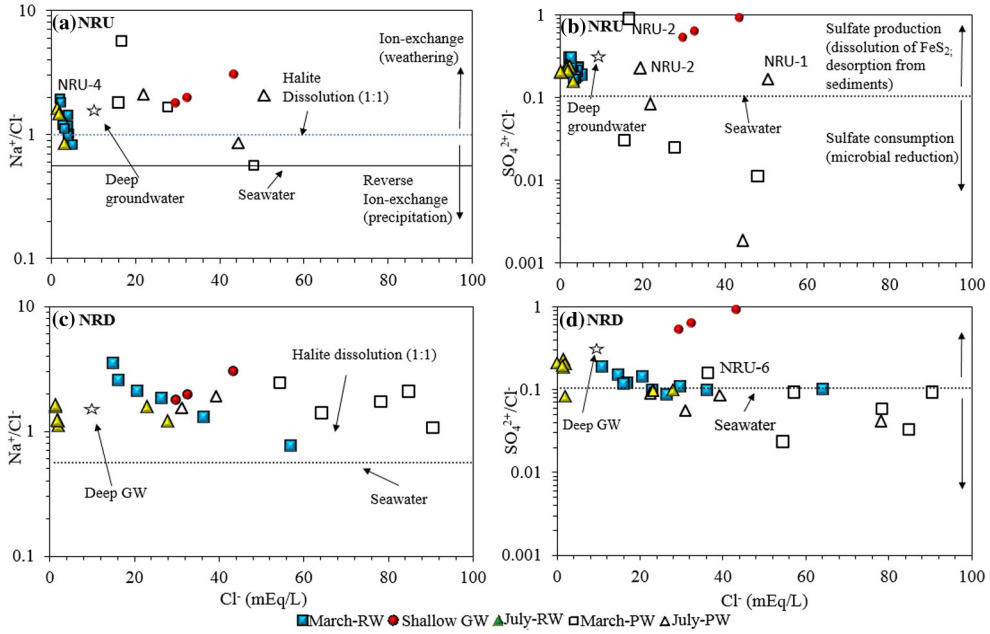

Fig. 5. Na^+/Cl^- and SO_4^{2-}/Cl^- molar ratios versus Cl^- concentrations (mEq/L) for the Nueces River upstream (a and b) and downstream (c and d) of the saltwater barrier dam. Deep groundwater is represented by average values. The characteristic Na^+/Cl^- ratio of halite dissolution and the seawater ratio are also represented.

likely as a result of lower inputs from benthic fluxes. Similar to the low flow conditions, production of SO_4^{2-} was still evident at NRU-2, and in addition at NRU-1, both located in close proximity to the near-bank wells sampled for this study (Fig. 1) which also showed high enrichment in SO_4^{2-}.

4.1.2.2. Downstream river. Porewater and surface water Na^+/Cl^- ratios in the downstream river were within similar ranges during both flow conditions with higher rates of Na^+ enrichment over chloride when compared to the seawater and halite dissolution ratios (Fig. 5c). On the other hand, in surface water the highest input of Na^+ from weathering of silicate minerals was more evident during low flow conditions when Na^+/Cl^- ratios reach the maximum average of 3.0 measured for both events in both stretches of the river (Table S1, Fig. 5c).

SO_4^{2-}/Cl^- showed in general a narrower range of values for the lower river, with values that for the most part plot closer to the seawater ratios (Fig. 5d). However, SO_4^{2-} consumption was noted for all porewaters during the low flow event, except for the furthest downstream location (i.e. station 6). Thus, the extent of SO_4^{2-} consumption was generally lower below the saltwater barrier. The potential for lower microbial activities was also supported by the lower DIC concentrations (Table S1) and somewhat enriched $\delta^{13}C$ ratios (Fig. 4b). On the other hand, slight enrichment in SO_4^{2-} to Cl^- in surface water was noted especially for the high flow event when the ratios increased to levels closer to the upstream river (Fig. 5b and d) which is the major source of inflow during this condition. More surface water samples showed seawater characteristics at low flow, although not at locations closer to the bay (Figs. 1, 5d).

4.1.3. Mixing endmembers

4.1.3.1. Cl^-/Br^- molar ratios and $\delta^{18}O$

4.1.3.1.1. Upstream river. During the dry weather, when river levels were at their lowest, the molar Cl^-/Br^- ratios of the upstream river- and pore- water (river water: 795 to 1112; porewater: 311 to 803) exceeded by far the seawater ratio characteristic of the area (i.e. discharging end-member bay ~626.2) (Fig. 6a). With one exception, surface water samples in this stretch of the river plot below and along the mixing lines between freshwater and deep groundwater and deep groundwater and halite dissolution. Although Cl^- is below the typical concentration of waters with chemistries influenced by halite dissolution, the Cl^-/Br^- ratios exceeding the marine ratio (i.e. ~ 780 mEq/L) with a slight change in Cl^- concentrations are an indication that this process may be occurring (Kloppmann et al., 2001). Na^+/Cl^- ratios showed that halite dissolution may occur but to a lesser extent then the weathering of silicate minerals (see Section 4.1.2). To note is that since input of Cl^- and Br^- from halite dissolution to surface water is dependent also on the benthic and groundwater fluxes witch vary along the river bed, a fairly similar increase in Cl^-/Br^- ratios and Cl^- should not be expected throughout.

With one exception, most porewaters plot in close proximity to the shallow groundwater and towards the deep groundwater fields (Fig. 6a). NRU-4 porewater with Cl^-/Br^- of 311 showed enrichment of Br^- with respect to Cl^- and exhibited the most depleted $\delta^{18}O$ (in porewater for this sampling event), a signature that can be associated with a more distant input of groundwater contaminated with fertilizer (Murgulet and Tick, 2013). The relationship between Cl^-/Br^- ratios and $\delta^{18}O$ abundances showed that slight effects of evaporation could be responsible for the higher Cl^- and Br^- concentrations of the porewaters (stations 4 to 6, i.e. Fig. 1) and in surface water at station NRU-2 (bottom and surface) (Fig. 6b). The rest of the surface water samples plot between the shallow groundwater and the deep groundwater-halite dissolution mixing line and away from the river/freshwater field (Cl^-/Br^- and Cl^-: 132 and 0.7 mEq/L, respectively).

During high flow conditions, Br^- concentrations for all but one NRU surface water samples were below the lower detection limit (i.e. 0.0006 mEq/L or 0.05 mg/L). Porewater Cl^- and Br^- concentrations were much more elevated at two of the four samples measured for this event compared to the low flow event while the other two were slightly lower (Table S1). The Cl^-/Br^- ratios showed similar characteristics to the shallow groundwater and plot further away from the deep groundwater mixing line when compared to low flow (Fig. 6a). Since the Cl^-/Br^- ratios only slightly changed, this increase was likely the effect of evaporation on the near-banks during the dry and low flow period preceding the high flow event. The more depleted $\delta^{18}O$ abundances of some of the porewater is indicative of groundwater input (deep and shallow) with Cl^-/Br^- signatures altered by mixing

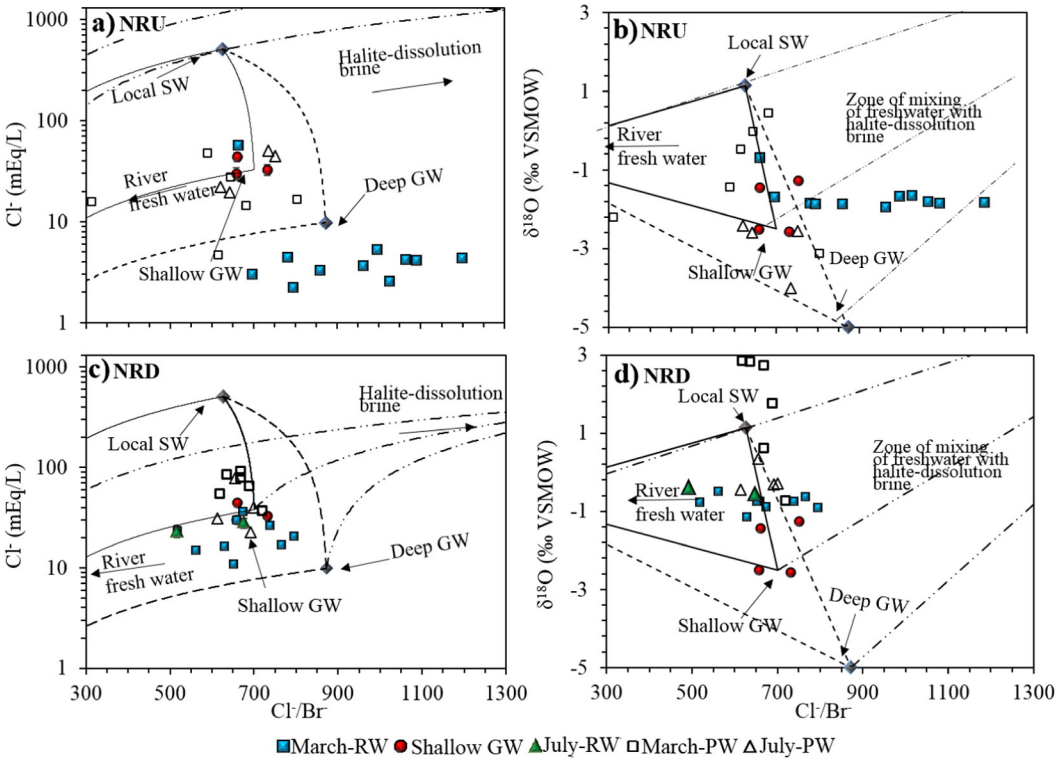

Fig. 6. Cross plots of Cl^- and $\delta^{18}O$ versus Cl^-/Br^- molar ratio of NRU (a and b) and NRD (c and d) porewaters, surface water and shallow groundwater (GW). Mixing lines between: river water-seawater and shallow groundwater (continuous lines); river water-halite-dissolution brine-shallow groundwater and deep groundwater (long dash dot dot lines); deep groundwater-seawater-river water (dash lines).

with ambient interstitial water and/or by evaporation effects (Fig. 6b). Thus, water chemistry was likely dominated by discharge from both bank storage and more distant groundwater, with the latter input increasing (i.e. more depleted $\delta^{18}O$ abundances in the July porewaters) as the drought progresses (Fig. 2) going from spring to summer.

4.1.3.1.2. Downstream river. In contrast to the upstream river, during low flow conditions, the Cl^- concentrations were much more enriched (average: 20.92 mEq/L) in the downstream water while the Cl^-/Br^- ratios followed a narrower range (517 to 795) and plot closer to the shallow groundwater field. At a few locations surface water Cl^-/Br^- ratios were lower than those of local seawater (Fig. 6c) indicating an enrichment in Br^- over Cl^-. Although more enriched in Cl^-, most porewaters showed more depleted Cl^-/Br^- ratios than groundwater and plot above the shallow groundwater-freshwater mixing line, within the freshwater-seawater-shallow groundwater field (Fig. 6c). Surface water has lower Cl^- concentrations and at most locations showed a significant decrease of the Cl^-/Br^- ratios below that of seawater indicating the possibility of halite precipitation. Halite formation takes up Cl^- while leaving the residual solution more enriched in Br^-, thus, with lower Cl^-/Br^- ratios (Cartwright et al., 2004). The input of waters with fertilizer signature (i.e. lower Cl^-/Br^- than seawater) is also likely as much of the area in the investigated catchment is agricultural.

The relationship between Cl^-/Br^- ratios and the $\delta^{18}O$ reveals greater effects of evaporation on the porewaters in this portion of the river (Fig. 6d) which was likely responsible for the increase in Cl^-. Most of the porewaters also fall under the zone of mixing between freshwater with halite-dissolution brine. The geochemistry of surface water was slightly affected by evaporation but precipitation and dissolution of halite may have also played an important role as revealed by Br^- levels which were depleted at some locations (i.e. halite dissolution) and enriched at others (i.e. halite precipitation).

At high flow, Br^- concentrations were detected at two locations in surface water. Porewater Cl^- and Br^- concentrations were overall lower than during low flow conditions (Table S1). The Cl^-/Br^- ratios showed similar characteristics to the shallow groundwater Fig. 6c) and lower effects of evaporation when compared to the low flow conditions (Fig. 6d). Mixing of freshwater with the ambient porewater should not alter the Cl^-/Br^- ratios unless it is accompanied by dissolution of halite as mentioned previously, but it will alter the $\delta^{18}O$ of water (i.e. a shift to more depleted abundances) as shown in this case. Given the lower land and river bank elevation in this part of the river as well as the characteristically low surface water levels (when compared to NRU), it is expected that during flooding events, such as those caused by environmental releases in July, surface water will invade the pore spaces within the hyporheic zone.

4.1.3.2. Saturation index (SI). Stability relationship analyses of river water, porewater, and groundwater showed that potassium (K^+)-feldspar and kaolinite were important controls on the chemical composition of water especially with respect to K^+, Aluminum (Al^{3+}), and silicate (SiO_4^{4-}) (Fig. S1). Thus, river water chemistry for both NRU and NRD stretches were controlled by weathering of silica-rich minerals such as K-feldspar. Weathering effects were also indicated by the enrichment of sodium over chloride (see Section 4.1.2) hinting at the possibility of albite (Na-rich feldspar) weathering. While no variation in the saturation indexes with respect to quartz and amorphous silica was observed for the two hydrologic conditions for the two river stretches (Fig. S1a), downstream water plots closer to the stability field of seawater (i.e. higher saturation with respect to quartz) while upstream waters showed more influence from weathering of aluminum oxides/hydroxides (i.e. kaolinite) (Fig. S1b). With higher H^+ activities, surface water and shallow groundwater were at equilibrium with K-feldspar while porewaters, with characteristically lower H^+ activities, were slightly undersaturated with respect to K-feldspar and more enriched in kaolinite. Generally through chemical weathering, K-feldspar breaks down into clay minerals such as kaolinite (Bergaya and

Lagaly, 2006). Porewater for both NRU and NRD fragments plots outside, or at the edge, of the stability field with seawater showing the effect of chemical weathering within the hyporheic zone (Fig. S1c).

4.1.3.2.1. Calcite saturation index and chloride mixing model. Saturation indexes calculated using PHREEQC offers a good understanding of the geochemical processes controlling the water as it uses the aqueous speciation of different elements and the likelihood of a certain mineral forming under equilibrium condition. As such, the saturation index with respect to calcium carbonate takes into account the ion activity and solid solubility products as dependent on the aqueous composition of major ions such as Al^{3+}, Mg^{2+}, Mn^{2+}, K^{+}, etc. All NRU and NRD pore- and surface- water were supersaturated with respect to calcium carbonate with higher saturation in the downstream (average: 1.4 for surface water and 0.5 for porewater) when compared to the upstream river (average: 0.9 for surface water and 0.4 for porewater) (Fig. 7). Shallow groundwater exhibited calcite saturation only slightly above the river- and pore- waters (average: 1.5) while deep groundwater showed a much lower saturation capacity (i.e. 0.01).

The SI–Cl^- mixing model calculations using PHREEQC showed that the interstitial water for both upstream and downstream river plot below the freshwater-seawater and freshwater-groundwater mixing lines (Fig. 7). Thus, calcite may be precipitating in the sediments. Assuming that groundwater is a source of bicarbonate alkalinity (average deep and shallow groundwater alkalinity: 6107 ($n = 6$) and 6879 ($n = 4$) mmol/L as bicarbonate, respectively), then calcite may be expected to precipitate in these sediments and could explain the lower SI than that of the shallow groundwater discharging laterally from bank storage. Furthermore, sulfate reduction was shown in this study to be substantial in some of the upstream sediments and in the downstream, although to a lesser extent (see Section 4.1.2). Microbial activity which can consume sulfate was shown to occur in these sediments also to a larger extent in the upstream stretch (see Section 4.1.1.2) (Andres et al., 2006). Thus, alkalinity can be produced within the sediments and facilitate the calcite precipitation (Larson et al., 1942).

Most NRU and NRD surface waters have calcite SIs exceeding that of seawater (i.e. 0.8) (Fig. 7) with a few exceptions of bottom waters that have lower indexes and close to the deep groundwater. While no indication of seawater input was revealed by these analyses (Fig. 7 a), groundwater contributions were significant. For instance, NRU river water signature was highly influenced by deeper groundwater chemistry (up to 40.3%) during the low flow conditions and to a lower extent (up to 20.0%) during high flow conditions (Fig. 7b, c). At high flow it is expected that the groundwater signature will be diluted with upstream river water and thus, lower the calcite SI. A slight contribution from shallow groundwater was estimated from these mixing models (up to 13.4% at low flow and 6% at high flow) which can be explained by dilution caused by: 1) upwelling of deep, less saturated groundwater; and 2) benthic fluxes of less saturated pore fluids which could be enhanced by the upwelling groundwater.

On the other hand, NRD surface water, which exhibited the highest calcite SI, showed a high influence of shallow groundwater (up to 83.3%) and no deep groundwater input (as dictated by Cl^- levels which were much more elevated when compared to deep water) at low flow while at high flow deep groundwater was higher (up to 17.0%) and shallow input was significantly lower (5.1%) (Fig. 7b, c). Contribution of deep groundwater during high flow in the downstream part of the river was likely derived from upstream discharge of water with a lower calcite SI and not from the upwelling of deep groundwater. Reduced shallow groundwater input could be explained not only by dilution from upstream discharges but also by the expected opposite gradients which likely favor groundwater recharge during high flow conditions, as indicated by the stable isotope investigations.

The mixing model estimates are in consent with ^{222}Rn concentrations measured in porewater and surface water showing a greater concentration in the upstream fragment when compared to the downstream one

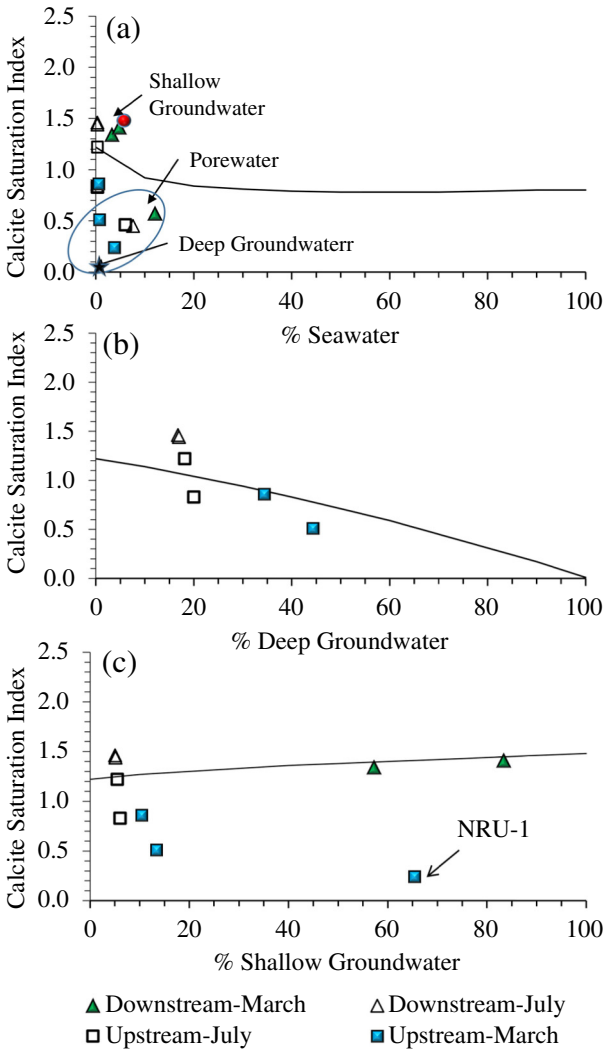

Fig. 7. Calcite saturation index and Cl^- mixing models for seawater (a), shallow groundwater (b), and deep groundwater (c) showing the estimated % contribution of the three sources to the NRU and NRD river waters. Note that porewaters are not shown in the groundwater plots because Cl^- concentrations exceed those of groundwater in most instances but one (i.e. March NRU-1) for the shallow groundwater end-member.

(Table S1). Concentrations of ^{222}Rn in the upstream porewater were in average 4801 Bq/m^3 at low flow and 4695 Bq/m^3 at high flow. Downstream these abundances were in average 2994 Bq/m^3 at low flow and 3907 Bq/m^3 at high flow. Surface water concentrations, although measured only at high flow in the upstream, showed that concentrations were much higher in average (555 Bq/m^3 at high flow) when compared to the downstream portion (average 212 Bq/m^3 at high flow). The one upstream measurement at high flow (155 Bq/m^3) was more elevated than the downstream average (58 Bq/m^3). These more elevated ^{222}Rn abundances in the upstream could be related to higher input of deep groundwater which was more enriched (average: 6976 Bq/m^3) than the shallow groundwater derived from bank storage (average: 3545 Bq/m^3).

4.2. Electrical resistivity

4.2.1. Continuous resistivity profiling

Inversion of the CRP files was constrained using fixed water resistivity (derived from point resistivity measurements using a direct-push probe) and thickness (collected using the GPS positioning system) to avoid overestimation or underestimation of the near-bottom resistivity. Orlando (2013) showed that these types of images can substitute

seismic data for the reconstruction of subsurface features and sedimentary characterization of near-bed sediments. The YSI resistivity values in the shallow groundwater samples along the southern flank of the upstream river ranged between 0.3 and 1.1 Ω-meter (Ω-m) (median 0.7 Ω-m). For the two surveys, the resistivity of the surface water varied significantly in both NRU and NRD segments (Table S1). Observed resistivity values in NRU were 6.9 Ω-m, on average, during the low flow conditions, and 13.0 Ω-m at high flow. A larger shift was observed for the downstream river where average resistivity values changed from 1.4 Ω-m, at low flow, to 14.5 Ω-m, at high flow. Thus the resistivity of the alluvium adjacent to the river may range from 0.3 to 14.5 Ω-m downstream of the dam and from 0.3 to 12.8 Ω-m upstream. These resistivities were in close agreement with the land ERT surveys as indicated in Section 4.2.2.

Point (YSI) porewater resistivity measurements in NRD increase from an average of 0.7 Ω-m at low flow to 3.0 Ω-m at high flow (Table S1). Low porewater resistivities are expected for the downstream river due to significant evaporation effects on the stagnant pools of water and recharging groundwater from near-bank storage during periods of droughts and limited or no upstream discharge. The effects of evaporation and the major input of shallow groundwater (i.e. hyporheic transport) were confirmed by the stable isotope and elemental geochemistry analyses as shown in the previous sections. As a result of evaporation the salinity content increases in both surface water and shallow groundwater and, due to density effects, more conductive pools of water settle/sink in the near-bottom and sediment pore spaces (Fig. S2; Supporting info.), thus interstitial fluid resistivity is decreasing.

Although the YSI pore measurements were consistent with high salt content composition of pore fluids, the CRP image collected during the same sampling period (i.e. low flow conditions) showed the existence of a more resistant layer near the sediment-water interface at multiple locations extending horizontally for several of hundreds of meters (see Fig. 8a, between NRD 3 and NRD-4). Nyquist et al. (2008) found that residuals clays saturated with freshwater can have an average resistivity of 38 Ωm while sandy clay loam will have an average resistivity 51 Ω-m. Because the YSI porewater resistivity measurements were on average lower than the direct current electrical resistivity measurements, it is likely that these layers of relatively lower conductivity are composed of sediments of higher permeability such as silty-sands or sand-clay loams that compose the hyporheic zone (Ward et al., 2010). The existence of hyporheic zones to extensive depths (up to 4 m) as identified in this study have also been found by Chen (2011). They also demonstrate that the existence of a hyporheic zone prevents regional or more distant groundwater discharge to streams, similar to the downstream fragment of this river. A layer of much lower resistivity (0.3 to 2.0 Ω-m) likely saturated with high salt content was present throughout the entire profile at an average depth of 5 m below the sediment-water interface (Fig. 8a).

In the upstream river, changes in the near-bed water chemistry were revealed by both CRP images and YSI porewater measurements collected for the two sampling events indicating the dynamic interaction between the river and groundwater in response to either drought or changes in hydrologic conditions. For instance, at low flow more extensive plumes of low resistivity were observed especially in close proximity to the Hazel Bazdemore Park (Fig. 8b) and the evaporation pond, a potential source of high salts to the groundwater and upstream river as shown by the land resistivity analyses (see Section 4.2.2 and Figs. S2 and S3) and the lower YSI resistivity of the porewaters (i.e. NRU-1 and NRU-2). Contamination of groundwater with high salts in close proximity to evaporation ponds has been documented by others (Chandler et al., 1985).

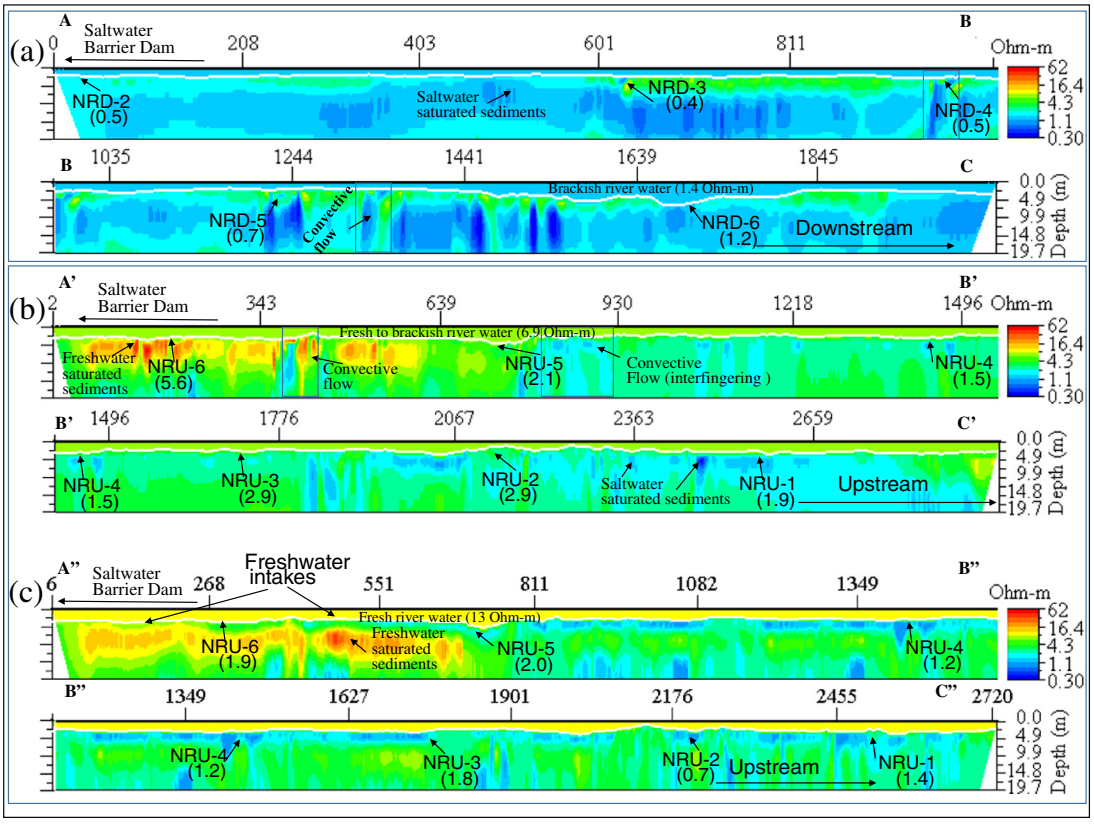

Fig. 8. CRPs of Nueces River downstream at low flow (a) and upstream at low flow (b) and high flow (c). The location of sampling sites and the corresponding porewater resistvity from YSI measurements is noted on the profiles. Note that the CRP A″–B″–C″ (c) is collected along the same line depicted in the inset picture in Fig. 1, at high flow in NRU. Also, important to note is the large differences in the subsurface resistivity in the sections adjacent to the saltwater barrier dam (left side of the first, third, and fifth panels) in the downstream (a) and upstream river stretches (b and c).

At high flow, the lower resistance plumes were much smaller, of lower resistivity, and mostly present in the near-bottom sediment. Changes in the near-bed interstitial water chemistry were complemented by the YSI measurements which showed that average porewater resistivities were decreasing from 2.8 Ω-m at low flow to 1.5 Ω-m at high flow (Table S1; Fig. 8c). These large observed variations in resistivities can be explained by density effects which cause the saltier water accumulated in the river during the prolonged period of drought (between the low and high flow conditions; see Fig. S2) to sink to the near-bottom sediments as the upstream freshwater inflows invade the river channel. Thus, the pore spaces become saturated mainly by more conductive fluids. Below these low resistance plumes which likely represent the hyporheic zone, porewaters become mostly occupied with fresh water that correlates well with an increase in upwelling of deeper groundwater as also indicated by the invasion of isotopically depleted water into porewater at high flow (see Section 4.1.1).

The CRP sections collected at low flow showed large differences in resistivity between the upstream and downstream imaged sections specifically below the hyporheic zone which may be more extensive downstream of the saltwater barrier (Fig. 8a, b). The first approximately 600 m upstream from the saltwater barrier showed the presence of a layer exhibiting the highest resistivity values measured in the study area (~20.0 to 62.0 Ω-m). While small decreases in resistivity were observed for this same section at high flow, values remain nearly above those measured throughout the rest of the sections. Measured YSI resistivity of the pore fluid was decreasing from 5.6 Ω-m at low flow to 1.9 Ω-m at high flow (Fig. CRP b1) indicating an input of saltier/brackish water between the two hydraulic conditions as indicated above. Inverted resistivities indicate that this layer continues further upstream but resistivities were much lower (~2.5 to 10.0 Ω-m). Changes in resistivity within this layer indicate that it is likely composed of higher permeability sediments such as sands and gravel associated with the central axis of the Nueces River meander belt (Fig. 1). Because the resistivity was decreasing within this layer between the low and high flow conditions, the fluid circulating through these permeable sediments was of different salinity content. Although of much lower resistivities (~0.3 to 2.5 Ω-m) the presence of this layer is also evident in the downstream river section. Since it is not expected that the sediment type and porosity/permeability of the subsurface to change abruptly just downstream the highly resistant section and the saltwater barrier, we believe that the sediments were saturated with high salt fluids.

4.2.2. Electrical resistivity land surveys

Resistivity imaging of the subsurface in both vertical and horizontal direction was conducted at the Hazel Bazemore Park near the shallow groundwater monitoring wells to complement geochemistry and water resistivity imaging investigations. Land resistivity profiles (using the EH4 Electrical Conductivity and Supersting R8/IP system) collected along a line extending from the evaporation pond to the river bank (Fig. 1) depict areas of low resistivity in close proximity to the river banks and near the pond (Fig. S3). The Supersting ERT showed a thin layer of low resistance near the land surface and a more resistant layer extending downward from ~2.5 m below land surface (Fig. S3) as also indicated by the NRU CRPs. The EH4 section, imaging to a depth of 200 m, showed that the low resistivity plume in close proximity to the pond may be spreading vertically to a depth of approximately 100 m below the surface and horizontally towards the river. Resistivity increases with distance from the pond (i.e. point source) as expected due to dilution effects.

Resistivity measurements of the shallow groundwater (within 5 m below the land surface) conducted using the EM 31 groundwater conductivity meter were acquired in the area surrounding the shallow groundwater wells and in close proximity to the evaporation pond (Fig. S4). These measurements, ranging from 0.8 to 27.3 Ω-m, resemble closely the YSI resistivities observed in the near-bank monitoring wells (average 0.5 to 1.1 Ω-m; average 0.6 Ω-m) and isolates the pond located just a few hundred meters west from the river as a potential local source of increased salinity in the near-river bank storage. Average YSI resistivity measurements of the pond surface- and pore- water (1.1 Ω-m) were in agreement with EM31 measurements and the effects of evaporation were also revealed by the enriched $\delta^{18}O$ and δD with average abundances (+1.7‰ and +6.8‰, respectively) exceeding or similar to average local seawater (+1.1‰ and +8.6‰, respectively). Porewater resistivity of samples NRU 1 and 2 located in the area identified as the discharge point of the saltier plume (Figs. 1 and S4) were generally the lowest in the upstream river (Table S1) constraining the resistivity imaging results and the input of groundwater from bank storage, laterally or within the hyporheic zone.

4.2.3. Continuous Rn and resistivity

Time-lapse ERT and continuous monitoring of ^{222}Rn and SC were conducted at station 6 to validate the high resistance layer identified by CRP images and the exchange between groundwater and river. The three time-lapse resistivity inversions collected at a time interval of 3.5 h were used to calculate % changes in the resistivity of porewater, and indicated changes in water chemistry as a result of groundwater-surface water interaction. Step-by-step analyses showed that a change of 6% occurred over the first time interval (T1–T2) while only 2% changes were measured during the second half (T2–T3) (Fig. S5a, b; Supporting info). Our data suggests the influx of water of higher resistance into the subsurface (~6 to 14 m below the sediment-water interface) (Fig. S5a: Supporting info) identified by the CRPs (Fig. 8b, c), for the first time interval. In spite of some inherent limitations of the electrical resistivity method (i.e. flushing of sediments with water of same or very similar salt content will result in very small % changes), the second time-lapse interval showed a slight change of the apparent resistivity towards less resistant fluids within the same zone.

Time-lapse resistivity changes were complemented by changes in ^{222}Rn and specific conductance in the overlying water which showed a decrease in water conductivity while ^{222}Rn levels were increasing to levels (~400 Bq/m^3) significantly above the lowest observed concentrations or background concentrations (~100 Bq/m3) during the first time interval (Fig. S5g; Supporting info). For the second interval, water conductivities increased slightly towards the end of the record while radon was considerably decreasing close to the minimum observed concentrations (~100 Bq/m3). Because ^{222}Rn is a gas and is rapidly lost to the atmosphere, high activities in surface waters are a strong indication of significant groundwater discharge (Moore, 2010). This confirms the interaction between groundwater and surface water and the input of fresher water upstream, near the saltwater barrier dam as shown by the CRPs (Fig. 8b and c).

5. Implication of barrier dams on the hydrogeochemistry of coastal rivers in semi-arid climates

Since the impact of barrier dams and regulated riverine inflows are recognized as a major issue around the world, with many more dams being constructed or planned for construction, investigation of hydrogeochemistry in the different fragments of these regulated rivers is necessary. This is essential for advancing understanding of the repercussions river regulation could have not only on hydraulic and biogeochemical functioning of the hyporheic zone, but on the availability and quality of water discharging to bays and estuaries. Here, we have shown through the combined application of elemental and stable isotope geochemistry and electrical resistivity imaging that river fragmentation caused by dams or barriers alter hydrological and geochemical processes affecting different parts of the river and the extents are likely amplified by climatic conditions.

For this study, the river fragment upstream of the saltwater barrier dam is dominated by groundwater upwelling from aquifers recharging further inland and, to lower extends, by hyporheic recharge. Microbial activities and weathering of silicate minerals are more significant in

this river fragment. Below the saltwater barrier, high river stages such as those caused by upstream environmental releases, are likely to cause downward fluxes of dense solute-concentrated waters deeper into the underlying aquifer. This river fragment receives very limited surface inflow but significant lateral recharge from bank storage through the hyporheic zone. Limited inflows and lower elevation of the area surrounding the tidal portion of the river (including the abandoned delta) favor formation of stagnant pools of water that are significantly affected by evaporation. Salts accumulating in the near banks, as a result of evaporation effects, are likely exchanged with the river through shallow subsurface transport. Groundwater discharge from bank storage through hyporheic exchange is a source of salts for both portions of the river, but the contribution is much lower upstream of the dam while much more significant downstream.

Porewater signatures observed for the low and high flow events, spanning over a period of drought and high temperatures, indicate that seasonal changes are likely occurring but are disturbed as a result of regulated inflows. At high flow, surface water signatures are dampened by upstream riverine inflows (i.e. dilution), possibly affecting some of the biological processes otherwise attuned to seasonal cycles of climate and flow dynamics. The response to such changes are expected to be more rapid and significant downstream of the dam, especially because of larger hydrological and geochemical alterations. This study presents an example application of methods and outcomes, but the techniques can be used to assess even larger spatial and temporal scales allowing for a comprehensive understanding of hydrologic alterations effects on rivers.

Supplement 1 shows Figs. S1, S2, S3, S4, and S5. Supplement 2 shows Table S1 summarizing all the geochemical parameters and YSI resistivity measurements. This material is available free of charge via the Internet at http://dx.doi.org/10.1016/j.scitotenv.2016.07.198.

Acknowledgments

This study was made possible with generous support from the LyondellBasell Industries and the Center for Water Supply Studies at Texas A&M University-Corpus Christi. We thank the numerous graduate and undergraduate students for assistance with field sampling efforts. Additionally, the Nueces River Authority provided generous resources instrumental to the completion of this work.

References

Alber, M., Flory, J., 2002. The Effects of Changing Freshwater Inflow to Estuaries: A Georgia Perspective. Georgia Coastal Research Council.
Andres, M.S., Sumner, D.Y., Reid, R.P., Swart, P.K., 2006. Isotopic fingerprints of microbial respiration in aragonite from Bahamian stromatolites Geology. 34, 973–976.
Arthington, A.H., 2012. History of water control and dam impacts. In: Arthington, A.H. (Ed.), Environmental Flows. Saving Rivers in the Third Millennium, 1 ed. University of California Press, pp. 87–98.
Ashworth, J., Hopkins, J., 1995. Aquifers of Texas: Texas Water Development Board Report 345. Austin.
Bauer, P., Supper, R., Zimmermann, S., Kinzelbach, W., 2006. Geoelectrical imaging of groundwater salinization in the Okavango Delta, Botswana. J. Appl. Geophys. 60 (2), 126–141.
Bergaya, F., Lagaly, G., 2006. General introduction: clays, clay minerals, and clay science. Handbook of Clay Science. 1, pp. 1–18.
Bighash, P., Murgulet, D., 2015. Application of factor analysis and electrical resistivity to understand groundwater contributions to coastal embayments in semi-arid and hypersaline coastal settings. Sci. Total Environ. 532, 688–701.
Burnett, W.C., 2003. Radon and radium isotopes as tracers in the coastal ocean. Abstr. Pap. Am. Chem. Soc. 226, U81.
Burnett, W.C., Dulaiova, H., 2003. Estimating the dynamics of groundwater input into the coastal zone via continuous radon-222 measurements. J. Environ. Radioact. 69 (1–2), 21–35. http://dx.doi.org/10.1016/S0265-931x(03)00084-5.
Cable, J.E., Martin, J.B., Swarzenski, P.W., Lindenberg, M.K., Steward, J., 2004. Advection within shallow pore waters of a coastal lagoon, Florida. Ground Water 42 (7), 1011–1020.
Cardenas, M.B., Markowski, M.S., 2010. Geoelectrical imaging of hyporheic exchange and mixing of river water and groundwater in a large regulated river. Environ. Sci. Technol. 45 (4), 1407–1411.
Cardenas, M.B., Zamora, P.B., Siringan, F.P., Lapus, M.R., Rodolfo, R.S., Jacinto, G.S., Diego-McGlone, S., Lourdes, M., Villanoy, C.L., Cabrera, O., 2010. Linking regional sources and pathways for submarine groundwater discharge at a reef by electrical resistivity tomography, 222Rn, and salinity measurements. Geophys. Res. Lett. 37 (16).
Cartwright, I., Weaver, T., Fulton, S., Nichol, C., Reid, M., Cheng, X., 2004. Hydrogeochemical and isotopic constraints on the origins of dryland salinity, Murray Basin, Victoria, Australia. Appl. Geochem. 19 (8), 1233–1254.
Chandler, R.V., Moore, J.D., Gillett, B., 1985. Ground-water Chemistry and Salt-water Encroachment, Southern Baldwin County, Alabama. Vol. 126. Geological Survey of Alabama, Water Resources Division.
Charette, M.A., Allen, M.C., 2006. Precision ground water sampling in coastal aquifers using a direct-push, shielded-screen well-point system. Ground Water Monit. Rem. 26 (2), 87–93.
Chen, X., 2011. Fluctuation of hyporheic zone thickness due to inflow and outflow across the water-sediment interface. Water Resource and Environmental Protection (ISWREP), 2011 International Symposium. vol 1. IEEE, pp. 388–391.
Chowdhury, A.H., Wade, S., Mace, R.E., Ridgeway, C., 2004. Groundwater availability model of the central gulf coast aquifer system: numerical simulations through 1999. Texas Water Development Board. 1, p. 14 unpublished report.
Cook, P.G., 2013. Estimating groundwater discharge to rivers from river chemistry surveys. Hydrol. Process. 27 (25), 3694–3707.
Craig, H., Gordon, L.I., 1965. Deuterium and Oxygen 18 Variations in the Ocean and the Marine Atmosphere.
Craig, H., Gordon, L., Horibe, Y., 1963. Isotopic exchange effects in the evaporation of water: 1. Low-temperature experimental results. J. Geophys. Res. 68 (17), 5079–5087.
Crusius, J., Koopmans, D., Bratton, J.F., Charette, M.A., Kroeger, K., Henderson, P., Ryckman, L., Halloran, K., Colman, J.A., 2005. Submarine groundwater discharge to a small estuary estimated from radon and salinity measurements and a box model. Biogeosciences 2 (2), 141–157.
Culkin, F., 1965. The major constituents of sea water. Chemical oceanography 1, 121–161.
Dynesius, M., Nilsson, C., 1994. Fragmentation and flow regulation of river systems in the northern 3rd of the world. Science 266 (5186), 753–762. http://dx.doi.org/10.1126/science.266.5186.753.
Feth, J.H., 1965. Preliminary map of the conterminous United States showing depth to and quality of shallowest ground water containing more than 1,000 parts per million dissolved solids. US Geol. Surv.
Francis, B.A., Francis, L.K., Cardenas, M.B., 2010. Water table dynamics and groundwater–surface water interaction during filling and draining of a large fluvial island due to dam-induced river stage fluctuations. Water Resour. Res. 46 (7).
Frei, S., Fleckenstein, J., Kollet, S., Maxwell, R., 2009. Patterns and dynamics of river–aquifer exchange with variably-saturated flow using a fully-coupled model. J. Hydrol. 375 (3), 383–393.
George, P.G., Mace, R.E., Petrossian, R., 2011. Aquifers of Texas. Texas Water Development Board.
Green, R.T., Winterle, J.R., Prikryl, J.D., 2008. Discharge from the Edwards Aquifer through the Leona River Floodplain, Uvalde, Texas1. Wiley Online Library.
Greenwood, W., Kruse, S., Swarzenski, P., 2006. Extending electromagnetic methods to map coastal pore water salinities. Ground Water 44 (2), 292–299.
Han, G., Liu, C.-Q., 2004. Water geochemistry controlled by carbonate dissolution: a study of the river waters draining karst-dominated terrain, Guizhou Province, China. Chem. Geol. 204 (1), 1–21.
Hellings, L., Van Den Driessche, K., Baeyens, W., Keppens, E., Dehairs, F., 2000. Origin and fate of dissolved inorganic carbon ininterstitial waters of two freshwater intertidalareas: a case study of the Scheldt estuary, Belgium. Biogeochemistry 51 (2), 141–160.
Jones, E.J., Nadeau, T.L., Voytek, M.A., Landa, E.R., 2006. Role of microbial iron reduction in the dissolution of iron hydroxysulfate minerals. J. Geophys. Res. Biogeosci. 111 (G1).
Kalbus, E., Reinstorf, F., Schirmer, M., 2006. Measuring methods for groundwater? Surface water interactions: a review. Hydrol. Earth Syst. Sci. Discuss. 10 (6), 873–887.
Kirtman, B.P.S.B., Adedoyin, J.A., Boer, G.J., Bojariu, R., Camilloni, I., Doblas-Reyes, F.J., Fiore, A.M., Kimoto, M., Meehl, G.A., Prather, M., Sarr, A., Schar, C., Sutton, R., Oldenborgh, G.J.V., Vecchi, G., Wang, H.J., 2013. Near-term Climate Change: Projections and Precidtability. (Cambridge, UK and New York, NY, USA).
Kloppmann, W., Négrel, P., Casanova, J., Klinge, H., Schelkes, K., Guerrot, C., 2001. Halite dissolution derived brines in the vicinity of a Permian salt dome (N German Basin). Evidence from boron, strontium, oxygen, and hydrogen isotopes. Geochim. Cosmochim. Acta 65 (22), 4087–4101.
Krishnaraj, S., Murugesan, V., Vijayaraghavan, K., Sabarathinam, C., Paluchamy, A., Ramachandran, M., 2011. Use of hydrochemistry and stable isotopes as tools for groundwater evolution and contamination investigations. Geosciences 1 (1), 16–25.
Kunze, H., 1971. Reconnaissance of the Chemical Quality of Surface Waters of the Nueces River Basin, Texas.
Larson, T.E., Buswell, A.M., Ludwig, H.F., Langelier, W., 1942. Calcium carbonate saturation index and alkalinity interpretations [with discussion]. J. Am. Water Works Assoc. 34 (11), 1667–1684.
Lee, D.R., 1977. A device for measuring seepage flux in lakes and estuaries. Limnol. Oceanogr. 22 (1), 140–147.
Li, X., Hu, B.X., Burnett, W.C., Santos, I.R., Chanton, J.P., 2009. Submarine ground water discharge driven by tidal pumping in a heterogeneous aquifer. Ground Water 47 (4), 558–568.
Lloyd, R., 1966. Oxygen isotope enrichment of sea water by evaporation. Geochim. Cosmochim. Acta 30 (8), 801–814.
Loke, M.H., 2011. Electrical Resistivity Surveys and Data Interpretation Encyclopedia of Solid Earth Geophysics. Springer, pp. 276–283.

Meybeck, M., 1987. Global chemical weathering of surficial rocks estimated from river dissolved loads. Am. J. Sci. 287 (5), 401–428.
Moore, W.S., 1996. Large groundwater inputs to coastal waters revealed by Ra-226 enrichments. Nature 380 (6575), 612–614. http://dx.doi.org/10.1038/380612a0.
Moore, W.S., 2010. The effect of submarine groundwater discharge on the ocean. Ann. Rev. Mar. Sci. 2, 59–88.
Moore, W.S., Church, T.M., 1996. Submarine Ground Water Discharge, Reply to Younger Nature. 382 p. 122.
Murgulet, D., Tick, G.R., 2013. Understanding the sources and fate of nitrate in a highly developed aquifer system. J. Contam. Hydrol. 155, 69–81.
NBBEST, N.R.a.C.C.a.B.B.B.a.B.E.S.T., 2011. Environmental flows recommendations report. Final Submission to the Environmental Flows Advisory Group, Nueces River and Corpus Christi and Baffin Bays Basin and Bay Area Stakeholders Committee, and Texas Commission on Environmental Quality.
Nyquist, J.E., Freyer, P.A., Toran, L., 2008. Stream bottom resistivity tomography to map ground water discharge. Ground Water 46 (4), 561–569.
Olden, J.D., Naiman, R.J., 2010. Incorporating thermal regimes into environmental flows assessments: modifying dam operations to restore freshwater ecosystem integrity. Freshw. Biol. 55 (1), 86–107.
Orlando, L., 2013. Some considerations on electrical resistivity imaging for characterization of waterbed sediments. J. Appl. Geophys. 95, 77–89.
Parkhurst, D., Appelo, C., 2005. PHREEQC-2 version 2.12: A hydrochemical transport model. US Geological Survey Central Region Research. USGS Water Resources Division http://www.brr.cr.usgs.gov/projects/GWC_coupled/phreeqc.
Parkhurst, D.L., Appelo, C., 2013. Description of input and examples for PHREEQC version 3: a computer program for speciation, batch-reaction, one-dimensional transport, and inverse geochemical calculations. US Geol. Surv.
Peterson, R.N., Burnett, W.C., Taniguchi, M., Chen, J.Y., Santos, I.R., Ishitobi, T., 2008. Radon and radium isotope assessment of submarine groundwater discharge in the Yellow River delta, China. J. Geophys. Res. Oceans 113 (C9).
Poff, N.L., Allan, J.D., Bain, M.B., Karr, J.R., Prestegaard, K.L., Richter, B.D., Sparks, R.E., Stromberg, J.C., 1997. The natural flow regime. Bioscience 47 (11), 769–784. http://dx.doi.org/10.2307/1313099.
Postel, S.L., 1998. Water for food production: will there be enough in 2025? Bioscience 48 (8), 629–637. http://dx.doi.org/10.2307/1313422.
Presley, B., Kaplan, I., 1968. Changes in dissolved sulfate, calcium and carbonate from interstitial water of near-shore sediments. Geochim. Cosmochim. Acta 32 (10), 1037–1048.
Price, R.M., Swart, P.K., Willoughby, H.E., 2008. Seasonal and spatial variation in the stable isotopic composition (δ 18 O and δD) of precipitation in south Florida. J. Hydrol. 358 (3), 193–205.
Richter, B.C., Kreitler, C.W., 1993. In: Smoley, K.C. (Ed.), Geochemical Techniques for Identifying Sources of Ground-Water Salinization 228. CRC Press, Boca Raton, Fl.
Richter, B.D., Thomas, G.A., 2007. Restoring environmental flows by modifying dam operations. Ecol. Soc. 12 (1), 12.
Richter, B.C., Kreitler, C.W., Bledsoe, B.E., 1991. Identification of Sources of Ground-Water Salinization Using Geochemical Techniques. US Environmental Protection Agency, Office of Research and Development, Robert S. Kerr Environmental Research Laboratory.
Rosenberg, D.M., McCully, P., Pringle, C.M., 2000. Global-scale environmental effects of hydrological alterations: Introduction. Bioscience 50 (9), 746–751. http://dx.doi.org/10.1641/0006-3568(2000)050[0746:Gseeoh]2.0.Co;2.
Samouëlian, A., Cousin, I., Tabbagh, A., Bruand, A., Richard, G., 2005. Electrical resistivity survey in soil science: a review. Soil Tillage Res. 83 (2), 173–193.
Sasamoto, H., Yui, M., Arthur, R., 1999. Status of Geochemical Modeling of Groundwater Evolution at the Tono in-Situ Tests Site, Japan. Japan Nuclear Cycle Development Inst.
Schmidt, D.H., Garland, K.A., 2012. Bone dry in Texas: resilience to drought on the upper Texas Gulf Coast. J. Plan. Lit., 0885412212454013
Sear, D., Armitage, P., Dawson, F., 1999. Groundwater dominated rivers. Hydrol. Process. 13 (3), 255–276.
Shafer, G.H., 1968. Ground-water resources of Nueces and San Patricio Counties, Texas. U.S. Geol. Surv.
Simmons, G., 1992. Importance of submarine groundwater discharge(SGWD) and seawater cycling to material flux across sediment/water interfaces in marine environments. Mar. Ecol. Prog. Ser. MESEDT 84 (2).
Simmons, C.T., Fenstemaker, T.R., Sharp, J.M., 2001. Variable-density groundwater flow and solute transport in heterogeneous porous media: approaches, resolutions and future challenges. J. Contam. Hydrol. 52 (1), 245–275.
Sparks, R.E., 1992. Risks of altering the hydrologic regime of large rivers. In J. Cairns, Jr., B. R.
Stevens, J.D., Sharp, J.M., Simmons, C.T., Fenstemaker, T., 2009. Evidence of free convection in groundwater: field-based measurements beneath wind-tidal flats. J. Hydrol. 375 (3), 394–409.
Su, N., Burnett, W.C., Eller, K.T., MacIntyre, H.L., Mortazavi, B., Liefer, J.D., Novoveská, L., 2012. Radon and radium isotopes, groundwater discharge and harmful algal blooms in Little Lagoon, Alabama. Interdisciplinary Studies on Environmental Chemistry. 6, pp. 329–337.
Swarzenski, P., Burnett, W., Greenwood, W., Herut, B., Peterson, R., Dimova, N., Shalem, Y., Yechieli, Y., Weinstein, Y., 2006. Combined time-series resistivity and geochemical tracer techniques to examine submarine groundwater discharge at Dor Beach, Israel. Geophys. Res. Lett. 33 (24).
USDI, 2000. Concluding report: Rincon Bayou demonstration project. In: Interior, U.D.o.t. (Ed.), Findings Volume II. US Department of the Interior, Bureau of Reclamation, Oklahoma-Texas Area Office, Austin, Texas.
Viso, R., McCoy, C., Gayes, P., Quafisi, D., 2010. Geological controls on submarine groundwater discharge in Long Bay, South Carolina (USA). Cont. Shelf Res. 30 (3), 335–341.
Walther, B.D., Nims, M.K., 2015. Spatiotemporal variation of trace elements and stable isotopes in subtropical estuaries: I. Freshwater endmembers and mixing curves. Estuar. Coasts 38 (3), 754–768.
Ward, A.S., Gooseff, M.N., Singha, K., 2010. Imaging hyporheic zone solute transport using electrical resistivity. Hydrol. Process. 24 (7), 948–953.
Weitkamp, L.A., 1994a. A Review of the Effects of Dams on the Columbia River Estuarine Environment, with Special Reference to Salmonids. Bonneville Power Administration.
Weitkamp, L.A., 1994b. A review of the effects of dams on the Columbia River Estuarine environment, with special refference to salmonids. 154.
White, P.A., 1988. Measurement of ground-water parameters using salt-water injection and surface resistivity. Ground Water 26 (2), 179–186.
Wooding, R., Tyler, S.W., White, I., 1997. Convection in groundwater below an evaporating salt lake: 1. Onset of instability. Water Resour. Res. 33 (6), 1199–1217.
Young, S.C., Pinkard, J., Bassett, R.L., Chowdhury, A.H., 2014. Hydrogeochemical Evaluation of the Texas Gulf Coast Aquifer System and Implications for Developing Groundwater Availability Models. Texas Water Development Board, Final Report # 1148301233: 375.